DR. GUILLERMO D. MAZZOLINI (Orcid ID : 0000-0001-7243-8077)

Article type : Original Articles

HE: Salvatore Pette

SPARC inhibition accelerates NAFLD-associated hepatocellular carcinoma development by dysregulating hepatic lipid metabolism

Agostina Mariana Onorato[1]; Esteban Fiore[1]; Juan Bayo[1]; Cecilia Casali[2,3]; María Fernandez-Tomé[2,3]; Marcelo Rodríguez[1]; Luciana Domínguez[1]; Josepmaría Argemi[4]; Florencia Hidalgo[5], Cristian Favre[5]; Mariana García[1]; Catalina Atorrasagasti[1*]; Guillermo D. Mazzolini[1,6*]

[1] Gene Therapy Laboratory, Instituto de Investigaciones en Medicina Traslacional, Facultad de Ciencias Biomédicas, CONICET- Universidad Austral, Av. Pte. Perón 1500 (B1629AHJ) Derqui-Pilar, Buenos Aires, Argentina.

[2]Universidad de Buenos Aires, Facultad de Farmacia y Bioquímica, Departamento de Ciencias Biológicas, Cátedra de Biología Celular y Molecular, Buenos Aires, Argentina.

[3]Universidad de Buenos Aires, Consejo Nacional de Investigaciones Científicas y Técnicas, Instituto de Química y Fisicoquímica Biológicas Prof. Dr. Alejandro C. Paladini (IQUIFIB)-Facultad de Farmacia y Bioquímica, Buenos Aires, Argentina.

[4]Josepmaria Argemi, CIMA and Clinica Universidad de Navarra, Pamplona, Spain.

[5]Institute of Experimental Physiology, CONICET, School of Biochemical Sciences, University of Rosario, Rosario, Argentina

This article has been accepted for publication and undergone full peer review but has not been through the copyediting, typesetting, pagination and proofreading process, which may lead to differences between this version and the Version of Record. Please cite this article as doi: 10.1111/LIV.14857

[6]Liver Unit, Hospital Universitario Austral, Universidad Austral, Av. Pte. Perón 1500 (B1629AHJ) Derqui-Pilar, Buenos Aires, Argentina.

*Both share credits for senior authorship

Correspondence: Guillermo D. Mazzolini, MD PhD. Liver Unit, Gene Therapy Laboratory, Instituto de Investigaciones en Medicina Traslacional, Facultad de Ciencias Biomédicas, CONICET- Universidad Austral, Av. Pte. Perón 1500 (B1629AHJ) Derqui-Pilar, Buenos Aires, Argentina. Phone: +542304387440; email: gmazzoli@austral.edu.ar

***Financial Support*:** this work was supported Austral University (T-13 for GM, T-14 for CA and T-13 for AO), Agencia Nacional de Promoción Científica y Tecnológica (ANPCyT) grant PICTO 2016/010 (GM), PICT 2018/03097 (CA), PICT 2018/ 4053 (GM), INC 2020 (GM).

***Disclosures*:** all authors declare that they have no conflict of interest.

Abbreviations: Adenovirus carrying SPARC antisense mRNA (**A**dasSPARC), Adenovirus carrying β-galactosidase (**A**d β-gal), Chow diet (CD), Differential gene expression (DEG), Dulbecco's modified Eagle's medium (DMEM), De novo lipogenesis (DNL), Extracellular matrix (ECM), Endoplasmic reticulum (ER), Fatty acid (FA), Fetal bovine serum (FBS), Neutral glycerophospholipids (GL-TAG), Gene onthology (GO), Glycerophospholipids (GPL), Hepatocellular carcinoma (HCC), High fat diet (HFD), International cancer genome consortium (ICGC), Mesenchymal to epithelial transition (MET), 3-(4,5-dimethylthiazol-3-yl)-2,5-diphenyltetrazodium bromide (MTT), Non-alcoholic fatty liver disease (NAFLD), Sodium acetate solution (NaOAc), NAFLD activity score (NAS), Non-alcoholic steatohepatitis (NASH), Oleate

acid (OA), Palmitic acid (PA), Phosphate buffer saline (PBS), Streptozotocin (SZT), The cancer genome atlas (TCGA), Triglycerides (TG).

Abstract

Background and aims: Non-alcoholic fatty liver (NAFLD) and its more serious form non-alcoholic steatohepatitis increase risk of hepatocellular carcinoma (HCC). Lipid metabolic alterations and its role in HCC development remain unclear. SPARC (Secreted Protein, Acidic and Rich in Cysteine) is involved in lipid metabolism, NAFLD and diabetes, but the effects on hepatic lipid metabolism and HCC development is unknown. The aim of this study was to evaluate the role of SPARC in HCC development in the context of NAFLD.

Methods: Primary hepatocyte cultures from knockout ($SPARC^{-/-}$) or wildtype ($SPARC^{+/+}$) mice, and HepG2 cells were used to assess the effects of free fatty acids on lipid accumulation, expression of lipogenic genes and *de novo* triglyceride (TG) synthesis. A NAFLD-HCC model was stablished on $SPARC^{-/-}$ or $SPARC^{+/+}$ mice. Correlations among SPARC, lipid metabolism-related gene expression patterns, and clinical prognosis were studied using HCC gene expression dataset.

Results: $SPARC^{-/-}$ mice increases hepatic lipid deposits over time. Hepatocytes from $SPARC^{-/-}$ mice or inhibition of SPARC by an antisense adenovirus in HepG2 cells resulted in increased TG deposit, expression of lipid-related genes, and nuclear translocation of SREBP1c. Human HCC databases analysis revealed that SPARC negatively correlated with genes involved in lipid metabolism, and with poor survival. In NAFLD-HCC murine model, the absence of SPARC accelerates HCC development. RNA-seq study revealed that pathways related to lipid metabolism, cellular detoxification, and proliferation were upregulated in $SPARC^{-/-}$ tumor-bearing mice.

Conclusions: The absence of SPARC is associated with an altered hepatic lipid metabolism, and an accelerated NAFLD-related HCC development.

Keywords: non-alcoholic fatty liver disease, secreted protein acid and rich in cysteine, lipid deposits, metabolism, sterol regulatory element-binding protein1c, hepatocellular carcinoma.

Lay Summary: In this study, we found that SPARC is involved in lipid metabolic modulation, the absence of SPARC increased liver fatty acid deposition and lipid metabolic pathways, contributing to hepatocellular development.

Introduction

Hepatocellular carcinoma (HCC) is the sixth most common cancer and the third leading cause of cancer-related death worldwide [1]. HCC is induced mainly by chronic hepatitis B and C virus, alcohol, and metabolic disorders such as nonalcoholic fatty liver disease (NAFLD). It is expected that the most common underlying cause of HCC in the world will be NAFLD, exceeding alcohol and viral-related cirrhosis [2]. NAFLD is currently the most common cause of chronic liver disease in developed countries [3,4]. NAFLD ranges from simple steatosis (NAFL) to more severe conditions such as steatohepatitis (NASH) and cirrhosis [5]. The incidence of HCC is rising steadily, and HCC is now a leading cause of obesity-related death in western countries [6]. Although NAFLD is a major global health problem, the molecular mechanisms underlying NAFLD-associated HCC remain unclear.

Altered lipid metabolism has been recognized as one of the hallmarks of cancer [7] as unrestricted lipogenesis provides cancer cells enough fuel for uncontrolled proliferation [8]. Recent evidence shows that metabolic changes in cancer cells increase carcinogenesis in murine obesity models [9]. Obesity and NASH are intimately related diseases [10]. Lipid metabolic reprogramming is recognized as an important issue in NASH-related HCC [11]. In line with this, HCC increased lipid biosynthesis has been reported to promote HCC development [12], whereas suppression of fatty acid (FA) biosynthesis pathway reduces HCC growth in murine models [13,14]. Inhibition of FA synthase (FASN) or acetyl-coA carboxylase (ACC), two key lipogenic enzymes, impair HCC cells growth [13]. Moreover, a recent study indicates that sterol regulatory element-binding protein 1 (SREBP1), a master regulator of lipogenic gene transcription, contributes to HCC progression [15]. In line with this, the suppression of SREBP1c in HCC cells induces growth arrest and apoptosis, whereas overexpression of SREBP1c increases cellular proliferation [16,17]. These findings suggest that increased lipogenesis is a driving force for HCC progression, although the molecular mechanisms behind the role of altered lipid metabolism in hepatocarcinogenesis remain poorly defined.

SPARC (secreted protein acidic and rich in cysteine) is a protein involved in different biological processes including tissue renewal, wound healing response to injury, tissue remodeling and fibrosis [18]. We and others previously described the role of SPARC in liver fibrogenesis [19–22]. In addition, increased hepatic expression of SPARC is associated with more pronounced liver injury and fibrosis in samples obtained from morbidly obese patients with NAFLD, and mice with diet-induced-NAFLD [23]. Interestingly, SPARC knockout mice fed with high fat and sucrose diet

increased liver steatosis indicating that the absence of SPARC is related with increased lipid deposition within hepatocytes. On the other hand, SPARC knockout mice displayed abnormal insulin-regulated glucose metabolism, presented increased adipose tissue deposition, and impaired glucose homeostasis [24].

We previously reported that SPARC overexpression reduced HCC tumorigenicity by inducing mesenchymal-to-epithelial transition (MET)[25]. However, the role of SPARC in HCC development in NAFLD context remains unknown. Endoplasmic reticulum (ER) stress response has recently been considered to play a crucial role in the development of NAFLD [26]. It has been recently demonstrated that SPARC is also localized within the endoplasmic ER, which has led to hypothesize that SPARC may act as an ER stress modulator [27]. SPARC acts as an enhancer of metabolism and a mediator of exercise-induced adaptation in skeletal muscle as well as an adipogenesis inhibitor in adipose tissue [28–30]. In addition, 5-aminoimidazole-4-carboxamide-1-β-D-ribofuranoside (AICAR)-stimulated AMPK phosphorylation is reduced by small interfering RNA of SPARC [31]. Interestingly, by co-precipitation assay Song *et al.* demonstrated that SPARC could interact with AMPK [31]. Several pieces of evidence implicated SPARC in metabolic and homeostatic roles, beyond the known ECM protein activity [32].

In the present study, we demonstrated that the absence of SPARC increases hepatic lipogenesis by increasing SREBP1c transcription and nuclear translocation and accelerates NAFLD-related HCC development. Importantly, in patients with HCC, SPARC negatively correlated with genes involved in lipid metabolism and with poor overall survival.

Materials and methods

Animals experimental design

In vivo experiments were performed in male C57BL/6J mice and SPARC knockout mice (SPARC$^{-/-}$) on a C57BL/6 background (Jackson Laboratory, USA). The STAM^{TM} mouse model was generated to study HCC development in NASH context. At 2 days of age mice were injected with a unique subcutaneous (s.c.) dose (200 μg) of streptozotocin (SZT) (Invitrogen). At week 4 we proceed to wean and separate them into 4 experimental groups: 1) SPARC$^{+/+}$ SZT fed *ad libitum* with high fat diet (HFD); 2) SPARC$^{+/+}$ SZT fed *ad libitum* with control laboratory chow diet (CD); 3) SPARC$^{-/-}$ SZT fed *ad libitum* with HFD; 4) SPARC$^{-/-}$ SZT fed *ad libitum* with CD [33]. All mice were euthanized after 16 weeks fed on the HF or control diet, and tumor size was evaluated. The HFD contains calcium caseinate (200 g/kg), vitamin mixture (10 g/kg), cellulose (50 g/kg), animal fat (250g/kg), vitamin A (1 ml/kg), choline bitartrate (2.5 g/kg), maltodextrin (451.5 g/kg). All protocols were reviewed and approved by the Austral University Animal Study Committee. This study followed the guidelines outlined in the National Institutes of Health Guide for the Care and Use of Laboratory Animals.

Primary hepatocyte isolation, HepG2 culture and in vitro *steatosis assay.*

Hepatocytes were isolated by collagenase perfusion[34] from 8-10 weeks-old SPARC$^{+/+}$ and SPARC$^{-/-}$ mice. Hepatocytes were growth in phenol red-free Dulbecco's modified Eagle's medium (DMEM) 10% fetal bovine serum (FBS). Two days after seeded, cells were incubated overnight (ON) with different concentrations (0.25, 0.5 or 1 mM) of free fatty acid (FFA), compound of a mixture 2:1 oleate acid (OA) and palmitic acid (PA) (Invitrogen) diluted in DMEM 10% FBS. Cells loaded with FFA were used for different experiments. Alternatively, cells were culture with 5 μg/ml 5-(Tetradecyloxy)-2-furoic acid (TOFA) (Sigma) plus FFA or with 2mM metformin (Sigma).

HepG2 human HCC cells were grown in DMEM 10% FBS. HepG2 cells, transduced with AdasSPARC[25] or Adβgal at MOI of 100; or non-transduced cells were used 48 h after infection. Cell loaded for 16 h with FFA were used for different experiments.

Quantitative real-time PCR

Cell culture or murine liver tumoral and non-tumoral tissue were homogenized, and total RNA was extracted using Trizol reagent (Sigma-Aldrich Co., USA). RNA (2 μg) was reverse

transcribed with 200 U of SuperScript II Reverse Transcriptase (Invitrogen, USA) using 500 ng of Oligo (dT) primers. cDNAs were subjected to qPCR. SPARC, PPARγ2, PPARα, CD36, FABP4, FABP5, ACC1, FASN, SREBP1, LxRα, CPT1, Lipin, ACADSB and ACOX1 mRNA levels were quantified by SYBR® Green (Invitrogen) qPCR (Stratagene Mx3005p, Stratagene, USA). All PCR amplifications were carried out using 40 cycles of 95 °C for 30 s, 55 °C for 30 s, and 72 °C for 30 s. Values were normalized to levels of 18S. Changes in gene expression were expressed as 2ΔΔCt referred to as fold change compared to the mean expression quantified in control group. See supplementary table 1 for list of oligonucleotides utilized for qPCR.

Pathological analysis

Liver tumoral and non-tumoral tissues were fixed in 10% formalin and embedded in paraffin. Hematoxylin and eosin liver specimens were evaluated by light microscopy. An experienced pathologist assessed steatosis, inflammation, and ballooning in a blinded fashion; and scored based on the NAFLD Activity Score (NAS) [35]. Pathologist was also consulted for determining tumoral areas inside liver parenchyma. For liver fibrosis assessment liver sections were stained with picrosirius red staining, and collagen fibers were quantified as described by Camino *et al*. [20]. Fresh liver tissue was frozen in optimal cutting temperature compound and stained with Oil Red O for lipid analysis [36].

Cell staining

Primary hepatocyte culture and HepG2 cells culture were also stained with Oil Red O for lipid analysis. Staining was quantified using the same criterion explained for picrosirius red staining. Alternately, the dye was extracted using 100% isopropanol, and absorbance was measured at 510 nm with a spectrophotometer to quantify the intracellular lipid content [37].

Immunofluorescence staining

For immunofluorescence studies of SREBP1c expression, primary hepatocyte or HepG2 cells were fixed in 4% paraformaldehyde, permeabilized with PBS-1% triton X-100, and blocked with 1% BSA in PBS-0.1% Tween for 15 min at room temperature, followed by an overnight incubation at 4°C in a humid chamber with a monoclonal mouse anti-SREBP1c antibody diluted 1:60 in PBS-0.1% BSA (Santa Cruz). After 3 washes with PBS, bound antibodies were detected with FITC or rhodamine-conjugated goat anti-mouse IgG (Jackson Immuno Research, West Grove, PA). Secondary antibody was diluted 1:40 in PBS-0.2% Tween and incubated for 2 h at

37°C. Nuclear morphology was examined by staining with DAPI. Images were captured from a Nikon E800 microscope coupled to a CCD camera.

Immunohistochemistry staining

For chromogenic immunohistochemical analysis and quantification of SREBP1 and PCNA expression, mice liver sections were deparaffinized and rehydrated. Antigen retrieval was carried out in a pressure cooker by boiling in 10 mM citrate buffer (pH 6.0), followed by washing with phosphate-buffered saline. Subsequently, endogenous peroxidase was quenched with 3% H_2O_2 for 20 min at room temperature. Thereafter, sections were subsequently blocked for endogenous biotin and avidin (Blocking kit, Vector Laboratories Inc.) 20 min each, and for unspecific binding of the primary antibody (1% BSA/PBS) 1 hour, always at RT. After rinsing, the slides were treated overnight at 4 °C with a negative control reagent or monoclonal mouse anti-SREBP1 (Santa Cruz) or PCNA antibody (Santa Cruz). After extensive washing, slides were incubated with peroxidase-linked biotinylated goat anti-mouse secondary antibodies for 1 h, washed and further incubated with AB complex at RT. They were then washed twice with PBS and twice with 0.1 M acetate buffer before incubation with a solution of 3.3-diaminobenzidine (DAB; Sigma), ammonium nickel sulfate and H_2O_2 until signal was developed. Primary antibody incubation was omitted in control slides, only rendering a faint staining (not shown). Positive cells were quantified using Image J (US National Institutes of Health, Bethesda, MD, USA) tool of cell count. Twenty random fields (200× magnification) were analyzed for each group.

Immunoblotting

Total proteins were separated by electrophoresis on SDS-polyacrylamide gels, and transferred to polyvinylidene difluoride membranes (Perkin Elmer Life Sciences, Boston, MA, USA). Membranes were blocked with 5% non-fat milk/0.3% Tween/PBS. Membranes were washed and incubated overnight with specific primary antibodies α tubulin (Sigma Chemical Co.) and Phospho-AMPKα (Thr172) (Cell Signaling Technology). Membranes were probed with the appropriate secondary antibody. Bands were detected by chemiluminescence (Amersham Pharmacia Biotech, Piscataway, NJ).

Metabolic labeling and lipid analysis

Lipid biosynthetic activity was determined as previously reported [38]. Briefly, lipid biosynthetic activity was evaluated studying the incorporation of the precursor [U-14C]-glycerol into

glycerophospholipids (GPL) and neutral glycerolipids (GL-TAG). Hepatocytes primary cultures were generated and grown for 48 h (70% confluence). Cultures were incubated with or without 0.5 mM FFA in DMEM 10% SFB for 16 h before lipid analysis. Then cells were incubated with 2 μCi/ml of [U-14C]-glycerol (PerkinElmer®) for 1, 2 and 3 h before harvesting. After counting, cells were washed in sterile PBS and subjected to lipid extraction. Lipid species were separated by thin layer chromatography (TLC). Different lipid species were identified by comparison with the corresponding standards and the retention factors. Radioactivity incorporated into glycerophospholipids (GPL) and fatty acids and neutral glycerolipids (GL-TAG) was visualized by radioautography and quantified by liquid scintillation counting.

Triglyceride quantification assay

Hepatic tissue samples of approximately (0.1 g) together with 1 ml of chloroform/methanol (2:1) solution were homogenized. The tubes were then centrifuged at 3000 rpm. An aliquot of chloroform/methanol extract was transferred to another tube and dried under a stream of nitrogen gas. These samples were dissolved in 100 μl isopropyl alcohol, after which cholesterol and triglyceride levels in the isopropyl alcohol were measured by conventional enzymatic methods (Wiener Lab, Rosario, Argentina).

Viability assays, cell proliferation and* in vitro *apoptosis assessment

Isolated primary hepatocyte cells ($3x10^3$) were seeded onto 96-well plates and treated with FFA as explain previously. Then, cells were incubated with 3-(4,5-dimethylthiazol- 3-yl)-2,5-diphenyl tetrazolium bromide (MTT, Promega) for 4 h at 37 °C. The formazan dye was solubilized and read at 490 nm optical density. Each assay was performed 3 times in triplicate and at least 4 independent experiments were performed. For the proliferation assay, primary hepatocyte cells ($8x10^3$/well) were incubated in a 96-well plate with FFA at different concentration and pulsed with 5 μCi/mL [methyl 3H] thymidine for 16 h. Then cells were lysed and the incorporation of radioactivity was measured in a liquid scintillation β-counter (Beckman Coulter, CA, USA).

Morphological changes associated with apoptosis were assessed by acridine orange-ethidium bromide mixture staining (Sigma). At least 100 cells were counted from 4 independent experiments and the percentage of alive, apoptotic and necrotic cells was determined. For quantifications, mean values from each independent experiment were normalized to their respective control values, prior to statistical comparisons.

Analysis of TCGA and ICGC cohorts

Clinical information and gene expression data (RNA sequencing [RNA-Seq]) were obtained from The Cancer Genome Atlas (TCGA) and International Cancer Genome Consortium (ICGC). HCC gene expression data for 377 (TCGA) or 203 (ICGC) patients with primary tumors who underwent tumor resection was obtained Data was transformed using the log2 (RSEM+1) formula. Expressed genes were correlated with SPARC expression. Genes were clustered by Pearson coefficient of correlation considering values equals or greater than 0.6 as strong positive correlation and less than -0.3 to -0.6, as moderate negative correlation. Above analyzes were performed using "R" software. GO (gene ontology) was analyzed in each gene clusters by ToppGene suit [39]. The patient clinical characteristics are shown in Table 1.

Overall survival of gene cluster was compared with the Log-rank test using GEPIA2 (RNA sequencing expression data of 9,736 tumors and 8,587 normal samples from the TCGA and the GTEx projects), group cutoff was set by quartile [15].

Transcriptome analysis of hepatic tissue from STAM murine model

Two independent animals were selected from the $SPARC^{+/+}$ and $SPARC^{-/-}$ experimental groups fed with HFD. RNA extraction was performed as previously described, from the liver sample containing neoplastic lesions. RNA was precipitated by adding 0.1 volumes of a 3M sodium acetate solution (NaOAc; pH 5.5) and adding 2 volumes of 100% ethanol. After performing quality control, qualified sample proceed to library construction (Illumina Truseq). RNA sequences (RNA-seq) were performed using the Illumina NextSeq 500 platform (Macrogen, Korea). For RNA-Seq analysis, R package Rsubread was used for the transcription assembly [40]. The edgeR package was used for feature counting and differential expression analysis between $SPARC^{+/+}$ and $SPARC^{-/-}$ mice. Genes were considered differentially expressed when log2 (fold change) was greater than 1 or less than -1 and p-value was <0.05. Functional gene set enrichment analysis including GO was performed using the Enrichr online tool [41].

Statistical analysis

Data are reported as arithmetic means ± SEM. All data were analyzed using Prism version 8 software (GraphPad, Carlsbad, USA). Statistical significance was determined with the appropriate test depending on data distribution and number of groups. Two-way ANOVA with Bonferroni correction for multiple comparison, one-way ANOVA Kruskal-Wallis test with Dunn's multiple

comparisons post-test, or the Mann–Whitney U-test were applied, respectively. For all analyses, a p-value <0.05 was considered statistically significant. For correlation analysis spearman rank correlation was applied.

Results

SPARC$^{-/-}$ mice show increased hepatic deposits of triglycerides in an age-dependent manner

It has been demonstrated that SPARC inhibits adipogenesis both in subcutaneous and visceral adipose tissue [42,43]. In line with this, we have previously observed that SPARC$^{-/-}$ mice develop hyperglycemia with age, and that a high fat diet increased body weight and liver steatosis in comparison with SPARC$^{+/+}$ mice [23,24]. To examine the time-dependent hepatic lipid deposits in the absence of SPARC, we performed a time-course observation in chow diet fed-SPARC$^{+/+}$ and SPARC$^{-/-}$ mice (from 6 to 30 weeks-old). Oil red hepatic tissue staining showed that SPARC$^{-/-}$ mice exhibited more TG (triglycerides) deposition than SPARC$^{+/+}$ in an age-dependent manner (Figure 1A). Quantitative measurement of TG in livers indicated significant TG accumulation in SPARC$^{-/-}$ mice from week 14 (Figure 1B).

SPARC knockdown is associated with increased lipid content in hepatocytes

Primary hepatocyte cultures were used to study the role of SPARC in lipid deposition. SPARC$^{-/-}$ hepatocytes had an increase in lipid droplets evaluated by oil red cell staining and oil red quantification by absorbance. *In vitro* culture of hepatocytes with increasing concentrations of free fatty acids (FFA) (OA/PA, 2:1 ratio) further increased lipid deposits in SPARC$^{-/-}$ hepatocytes compared with SPARC$^{+/+}$ (Figure 2A-B). Consistently, chromatography of cell-extracted lipid analysis revealed an increased amount of endogenous neutral triglycerides (GL-TAG), although no significant differences were observed in the glycerophospholipid (GPL) content (Figure 2C).

Then, to study whether increased FFAs can exert a different effect on hepatocytes depending on the expression of SPARC, we employed a recombinant adenovirus carrying SPARC antisense mRNA (AdasSPARC) or, alternatively, expressing β-galactosidase as a control (Adβgal) in HepG2 cell line. SPARC expression was decreased near 60% in AdasSPARC-treated HepG2 cells compared with Adβgal-treated cells (Figure 2D). Then, HepG2 cells were cultivated in the presence or absence of FFA for 12 h. As expected, wild type HepG2 increased lipid deposition when they were co-cultured with 0.5 mM or 1mM FFA. On the contrary, SPARC inhibition increased lipid droplets deposition (AdasSPARC vs. Adβgal), both in the presence and absence of

FFA (Figure 2E). These results suggest that the hepatic expression of SPARC is linked with the lipid deposits within hepatocytes.

SPARC$^{-/-}$ hepatocytes exhibit increased triglyceride synthesis

To differentiate hepatocyte lipid deposition from an increase in lipid uptake and/or an increase in *de novo* lipogenesis (DNL) we first measured *de novo* TG synthesis. Hepatocyte primary cultures were obtained from SPARC$^{+/+}$ and SPARC$^{-/-}$ mice, and incorporation of ^{14}C- glycerol into GL-TAG during 1, 2 or 3 h was measured. We did not find significantly differences in TG-kinetic synthesis between SPARC$^{+/+}$ and SPARC$^{-/-}$ hepatocytes. However, when hepatocytes were pre-incubated in the presence of 0.5 mM FFA for 16 h, we found that SPARC$^{-/-}$ hepatocytes increased *de novo* TG synthesis in comparison with SPARC$^{+/+}$ hepatocytes, showing an increase in TG-kinetic synthesis (Figure 3A). Interestingly, FFA-treated SPARC$^{-/-}$ hepatocytes showed a greater *de novo* TG synthesis after only 1 h in comparison with SPARC$^{+/+}$ hepatocytes (Figure 3A). To exclude the possibility that the increased TG synthesis observed in the absence of SPARC was due to increased FFA uptake and not because of an increment in FFA synthesis, we examined neutral lipid accumulation in the presence of TOFA, an inhibitor of the synthesis of malonyl-CoA by acetyl-CoA carboxylase (ACC). Thus, we measured the increment in hepatocyte GL-TAG accumulation induced by FFA in the presence or absence of TOFA. No significant difference in neutral lipid deposition was observed between SPARC$^{+/+}$ and SPARC$^{-/-}$ hepatocyte when TOFA was used (Figure 3B). These data suggest that the increased TG synthesis previously observed in SPARC$^{-/-}$ is probably due mainly to an increment in the synthesis of TG and not because of increased FFA uptake.

SPARC absence stimulates hepatic lipid metabolism via up-regulation of lipogenic enzymes

To study the role of SPARC in the regulation of hepatic lipid metabolism, we analyzed the expression of key lipogenic enzymes and fatty acid transporters including ACC1, FASN, PPARα, PPARγ2, CD36, FABP4, and FABP5 in primary hepatocyte cultures (with or without FFA), and in hepatic tissue from SPARC$^{+/+}$ and SPARC$^{-/-}$ mice. Interestingly, SPARC$^{-/-}$ hepatocytes showed increased expression of lipid transporters (CD36, FABP4, FABP5), genes involved in FA synthesis (ACC1, FASN), TG synthesis (LIPIN1) and β-oxidation (CPT1, ACOX1) compared with SPARC$^{+/+}$ (Figure 3C). It is well established that lipogenic enzymes genes are commonly trans-activated by sterol regulatory elementary binding protein 1 (SREBP1), an essential transcription factor for regulation of fatty acid synthesis. We studied the gene expression

SREBP1c because it is the dominant isoform in normal liver and HCC [44]. We observed that SREBP1c showed a significant increased expression in SPARC$^{-/-}$ hepatocytes (fold change 3.75±0.53, p=0.002 SPARC$^{-/-}$ vs SPARC$^{+/+}$) (Figure 3C), suggesting that SPARC regulation of lipogenic enzymes, could be mediated by changes in the SREBP1c gene expression and/or SREBP protein activation. Metabolic transcription factors, such as PPARγ2, PPARα and LXRα, were also upregulated in SPARC$^{-/-}$ hepatocytes, although in less amount. No significance differences were observed in ACADSB gene expression (Figure 3C).

The absence of SPARC is associated with increased metabolic and proliferative activity in hepatocytes in response to FFAs

To assess whether the lipogenic phenotype induced by SPARC inhibition might affect HCC proliferation, as a feature of cell aggressiveness, primary hepatocyte culture cells were incubated with or without FFAs, and cell viability was evaluated by MTT assays. MTT assay allows assessing not only cell viability but also metabolic activity by measuring NAD(P)H-dependent cellular oxidoreductase activity. SPARC$^{-/-}$ hepatocytes increased their metabolic activity and viability when compared to SPARC$^{+/+}$ hepatocytes (Figure 3D). In line with this results, we observed that SPARC$^{+/+}$ hepatocytes incubated with 1mM FFAs decreased their proliferative activity compared with SPARC$^{+/+}$ hepatocytes without FFAs, while proliferative activity was not affected in FFA-treated SPARC$^{-/-}$ hepatocytes (Figure 3E). Moreover, apoptosis was also assessed by acridine orange-ethidium bromide staining (Figure 3F). The assay shows no change in the number of live cells when in SPARC$^{+/+}$ and SPARC$^{-/-}$ hepatocyte incubated with 0.25 mM and 0.5 mM FFAs (data not shown), however, 1mM FFA-incubation decreased cell viability and increased apoptotic events in SPARC$^{+/+}$ hepatocytes but not in SPARC$^{-/-}$ hepatocytes. These results suggest that SPARC$^{-/-}$ hepatocytes may acquire a more aggressive phenotype in the presence of FFA by showing more proliferative phenotype, FFA activated-metabolic activity and resistance to apoptosis.

The absence of SPARC increased SREBP1c nuclear translocation

SREBPs is first synthesized as an inactive precursor that is bound to endoplasmic reticulum (ER)[45]. After a cleavage process, these inactive precursors are processed into an activated mature SREBPs, which in turn translocate to the nucleus, resulting in transactivation of downstream targets involved in lipogenesis [46]. To elucidate whether SPARC could be involved in SREBP1c activation, we first performed immunofluorescence staining for SREBP1c in primary hepatocyte

culture as well as in HepG2 cells to assess its localization. We observed predominant cytoplasmic and perinuclear SREBP1c localization in SPARC$^{+/+}$ hepatocytes in the absence of FFA, while SREBP1c was translocated to the nucleus when FFAs were added (Figure 4A-B). In contrast, SREBP1c had a nuclear localization in SPARC$^{-/-}$ hepatocytes both in the absence and presence of FFA (Figure 4A-B). Similar results were obtained in HepG2 cells (Figure 4C-D). SPARC inhibition increased the number of cells with nuclear SREBP1c localization compared with Adβgal-treated HepG2. As expected, FFAs induced nuclear localization. Then, we performed immunohistochemistry on liver tissue from SPARC$^{+/+}$ and SPARC$^{-/-}$ mice and confirmed that SREBP1c had a predominant nuclear localization in the absence of SPARC (Figure 4E).

It has been previously observed that SPARC can interact and activate AMPK [31,47]. The activation of AMPK then phosphorylates SREBP blocking its nuclear translocation. To test whether SPARC could regulate SREBP1c localization in hepatocyte, we evaluated AMPK activation in SPARC$^{+/+}$ and SPARC$^{-/-}$ hepatocyte primary culture. AMPK activation was significantly inhibited in SPARC$^{-/-}$ hepatocytes as observed by the reduction of p-AMPK (Figure 4F).

Metformin is a widely used antidiabetic drug that exerts a strong inhibitory effect on lipogenesis. Metformin activates AMPK, which in turn phosphorylates SREBP1c, and inhibits nuclear translocation [48]. To explore if we can revert the nuclear translocation of SREBP1c in the absence of SPARC, we incubated hepatocytes with metformin and demonstrated that SREBP1c nuclear localization is lost in metformin-treated SPARC$^{-/-}$ hepatocytes, suggesting that SPARC effects on SREBP1c cellular location could be mediated by modulation of AMPK activity (Figure 4G).

SPARC inhibition is associated with altered lipid metabolic profile in HCC human samples

To explore whether SPARC is involved in the regulation of aberrant lipid metabolism in HCC, we performed both bioinformatic analyses in human samples and in a murine HCC model. First, we asked which type of genes correlate with SPARC expression. TCGA and ICGC datasets of RNAseq in HCC were obtained, and the ToppGene biological process enrichment analysis was then performed. We found 490 genes that positively correlated with SPARC expression in TCGA dataset, while 404 genes were found in ICGC dataset. 299 genes were shared between both datasets (Figure 5A). In both datasets we observed that genes that positively correlated with SPARC expression were involved in extracellular matrix organization, vasculature development, response to wounding, cell adhesion and migration (strong positive correlation, Pearson coefficient ≥0.6)) (Figure 5B). Next, we analyzed those genes which negatively correlated with

SPARC expression, and obtained a gene cluster of 207 and 312 genes that correlated negatively with the expression of SPARC in TCGA or ICGC datasets, respectively (Person correlation between -0.3 and -0.6). Both datasets shared 54 genes (Figure 5A). Interestingly, the ToppGene analysis of TCGA and ICGC genes clusters showed metabolic-related biological processes which clearly inversely correlated with SPARC. Genes related to small molecule catabolic process, organic acid and carboxylic metabolic process, lipid homeostasis, lipid biosynthesis lipid metabolic and carboxil acid metabolic processes were identified (Figure 5C). This data suggests that SPARC might play a key role in lipid metabolism in HCC. Therefore, to determine the importance of these pathways in hepatocarcinogenesis, we did a survival analysis using the 207 genes of TCGA cluster as a signature. The Kaplan-Meir and Cox proportional hazards analyses showed that high expression of the gene signature was associated with poor patient survival (Figure 5D), suggesting that increased expression of SPARC-inhibited metabolic and lipid metabolic-related genes are associated with HCC progression.

The absence of SPARC increases steatosis and promotes hepatocarcinogenesis in a NAFLD-related HCC in mice

To test the role of SPARC in NAFLD-related HCC, we used a murine model of streptozotocin-induced NASH-HCC model (STAM model). The STAM protocol produces fatty liver, NASH, fibrosis and HCC under diabetic conditions [33,49,50]. Histopathologic analysis of liver tissue from 8-week-old mice revealed that both SZT-HFD fed $SPARC^{+/+}$ and $SPARC^{-/-}$ presented hepatic damage (NAS score 4.8±0.65 and 4.14±0.4, respectively). However, SZT-HFD fed $SPARC^{-/-}$ had a significantly higher steatosis degree compared with SZT-HFD $SPARC^{+/+}$ mice (2.6±0.27 vs 1.57±0.2, $p<0.5$) but lower lobular inflammation (1.33 ± 0.52 vs 2.0 ± 0.00, $p<0.5$) (Figure 6A-B). On the contrary, SZT-HFD fed $SPARC^{+/+}$ reached a similar NAS score than SZT-HFD fed $SPARC^{-/-}$ by increasing inflammation. SPARC expression was significantly increased during NAFLD progression (Figure 6C). H&E staining also showed less portal inflammation (Figure 6A) as well as a decreased of pro-inflammatory cytokines and chemokines such as IL-6, TNFα, IP10, IL1β expression in SZT-HFD fed $SPARC^{-/-}$ compared with $SPARC^{+/+}$ mice (Figure 6D). Then, we measured inflammasome activation by expression analysis of NLRP3 and CASP1, the two key molecules which trigger the cleavage of IL1β. Interestingly, SZT-HFD fed $SPARC^{-/-}$ had reduced expression of these genes (Figure 6D). To study the effects on fibrogenesis in $SPARC^{-/-}$ and $SPARC^{+/+}$ mice, Sirius red staining was performed. As expected, SZT-HFD fed $SPARC^{+/+}$ mice

presented mild perisinusoidal fibrosis. Notoriously, SZT-HFD fed SPARC$^{-/-}$ presented less collagen deposits compared to SZT-HFD fed SPARC$^{+/+}$ (Figure 6F).

Next, we examined the oncogenic potential of SPARC. At week 16, both SPARC$^{-/-}$ and SPARC$^{+/+}$ mice developed HCC (figure 7A-B). Tumors greater than 1 mm^3 were macroscopically counted. The volume of each nodule was also measured, and the tumor burden was calculated for each liver. SPARC$^{-/-}$ and SPARC$^{+/+}$ mice did not significantly differ in the number of HCC nodules, although a nominally increase was observed in SPARC $^{-/-}$ mice after 16 weeks (Figure 7C). Interestingly, tumor burden was higher in SPARC$^{-/-}$ mice (123.6±35.26 vs 313.9±71.79, $p \leq 0.0001$) (figure 7D). Mice lacking SPARC had increased tumor incidence both for ≤ or > a 1 mm^3 tumors (Figure 7E). Because hyperproliferation is a common phenotype in hepatocyte transformation, we evaluated proliferation in tumor and adjacent-tumor tissue by immunohistochemical staining for PCNA. Compared to SPARC$^{+/+}$ mice, SPARC$^{-/-}$ had evidence of hyperproliferation (Figure 7F-G). Taken together these results strongly suggest that the absence of SPARC is linked to an increased HCC development in mice with NASH.

SPARC absence is associated with altered lipid metabolic pathways in murine NAFLD-related HCC

Finally, we performed a transcriptome profiling of HCC in mice lacking SPARC by analyzing liver tissues containing hepatic tumors from SZT-HFD fed SPARC$^{-/-}$ and SPARC$^{+/+}$ mice. Differential gene expression (DEG) patterns were analyzed. We found 1658 differentially expressed genes between samples from SPARC$^{-/-}$ and SPARC$^{+/+}$ mice. In line with *in vivo* results, pathway enrichment analysis of DEGs genes in SPARC$^{-/-}$ mice revealed that they are involved in epithelial mesenchymal transition, DNA replication and maintenance, cell cycle and mitosis. Moreover, pathway enrichment analysis showed modulation of metabolic pathways (Figure 7H, left plot). Then, we focused our analysis in DEG with a fold change greater than 2 or less than 0.5. 302 genes were upregulated in SPARC$^{-/-}$ tissue (fold change ≥2, $p \leq 0.05$), and 355 downregulated (fold change ≤ 0.5, $p \leq 0.05$), in SPARC$^{-/-}$ samples compared with SZT-HFD SPARC$^{+/+}$ mice (Figure 7H). Pathway enrichment analysis of significant upregulated genes in SPARC$^{-/-}$ were related to diverse metabolic pathways (Figure 7H, right plot), such as estrogen metabolism, nuclear receptors in lipid metabolism or fatty acid omega oxidation. These results are in agreement with increased hepatocyte proliferation observed in the STAM model. Overall, these results are in line with the direct connection of SPARC with lipid metabolism, and with the association of

SPARC deficiency with increased risk of HCC development in NAFLD context seen in the *in vivo* and *in vitro* experiments.

Discussion

In this work, we demonstrated that the absence of SPARC increases lipid deposition in hepatocytes, and that SPARC has a pivotal role in regulating lipid metabolism in the liver. $SPARC^{-/-}$ hepatocytes showed increased lipid droplet content and higher expression of lipid transporter genes (CD36, FABP4, FABP5), lipogenic genes (FASN, ACC1, SREBP1), and genes involved in β-oxidation and TG synthesis (LIPIN1). Moreover, increased de novo TG synthesis was observed in $SPARC^{-/-}$ hepatocytes. We further investigated the effects of lipid overload in hepatocytes and observed that $SPARC^{-/-}$ hepatocytes showed higher cell viability, proliferation, and resistance to apoptosis in the presence of high FFA concentrations in comparison with $SPARC^{+/+}$ mice. Finally, we demonstrated that the absence of SPARC accelerates HCC development in NAFLD-HCC model. RNA-seq study revealed that pathways related to lipid metabolism, cellular detoxification, and proliferation were upregulated in $SPARC^{-/-}$ tumor-bearing mice.

SPARC is expressed in several tissues exerting a variety of remodeling and metabolic functions [32]. In adipose tissue, SPARC inhibits adipogenesis likely due to the stimulation of the Wnt/β-catenin signaling pathway which in turn cause inhibition of adipogenic transcription factors including CAAT/enhancer-binding protein α (C/EBPα), CAAT/enhancer-binding protein β (C/EBPβ), and peroxisome proliferator-activated receptor γ (PPARγ)[51]. In skeletal muscle, SPARC acts as a metabolism enhancer and a mediator of exercise-induced adaptation [52]. On the other hand, $SPARC^{-/-}$ mice show severe glucose homeostasis alterations with age and after high fat diet conditions [24]. Therefore, the observed increase in lipid deposits may be the result of an unbalanced energy state related with high glucose levels [24] or elevated FFA levels as a consequence of augmented adipogenesis [42]. Besides, here we showed an intrinsic effect of SPARC in cell metabolism since *in vitro* assays for SPARC inhibition in HepG2 showed changes in neutral lipid deposits.

SREBP1-mediated lipogenic pathway and high SREBP1c expression is associated with poor prognosis in HCC[53]. Moreover, inhibition of SREBP1c nuclear translocation inhibits DEN-induced HCC growth[16]. We observed in our work that the absence or the inhibition of SPARC increases SREBP nuclear localization in hepatocytes, which was further reverted by metformin. Metformin targets AMPK and increases AMPK activation by phosphorylation, which in turn block SREBP nuclear translocation[54]. SPARC may interact with AMPK, SPARC effects on

SREBP cellular location could be mediated by modulation of AMPK activity. Here we reported that in the absence of SPARC, AMPK activation was clearly reduced. By yeast-two hybrid and co-immunoprecipitation assays in HepG2 and hepatic tissue, Song *et al.* showed that SPARC is an AMPK-interacting protein and may be involved in regulating metabolism via AMPK activation[31]. Thus, SPARC may interact directly or indirectly with AMPK preventing its activation thus regulating lipid metabolism.

One of the most important metabolic hallmarks of cancer is enhanced lipogenesis[55]. Fatty acids promote several features related to cancer cell development, progression, and survival [8]. Changes in lipogenesis start early during carcinogenesis and further expands as the tumor cells become more aggressive. Dysregulation of lipid metabolism and accumulation of TG in the liver are key events in NAFLD, a disease with increases the risk of HCC development. Lipid metabolic reprogramming is recognized as an important issue in NASH-related HCC[11]. Therefore, identifying new pathways involved in hepatocarcinogenesis in the context of NAFLD is needed. To further investigate SPARC-mediated metabolic alteration in a NAFLD context, we used the NAFLD-HCC STAM model [33,50] in SPARC$^{-/-}$ mice. The lack of SPARC resulted in accelerated hepatic lipid deposition, although increased steatosis was not associated with inflammation and fibrosis when compared with SPARC$^{+/+}$ mice. This result was in concordance with our previous report in a diet-induced obesity NAFLD murine model [24]. Then, we evaluated HCC development after 16-weeks, and observed that SPARC$^{-/-}$ mice showed accelerated HCC growth. In line with this, we have previously reported that SPARC overexpression in HCC cells result in a reduced tumorigenicity when inoculating subcutaneous in nude mice, partially through the induction of mesenchymal-to-epithelial transition [25]. To our knowledge, this work studies for the first time the role of SPARC in NAFLD-related HCC. Herein we showed that HCC development is increased in SPARC$^{-/-}$ mice and it was associated with reduced inflammation and fibrosis degree in the livers. Our findings could be important considering that the incidence of HCC in obese patient with steatosis is steadily increasing [6]. One limitation of our study is that mice in the STAM model, although develop HCC in a short time, are lean and in contrast to human with NASH-related HCC which occurs, in most cases, in an obese context, with insulin resistance and type 2 diabetes mellitus. In addition, SZT could have an independent carcinogenic effect on hepatocytes, given that it has been reported as a DNA-damaging alkylating agent [56]. Despite these considerations, SZT/HFD-treated SPARC$^{-/-}$ mice showed an increased HCC development in comparison with SZT/HFD-treated SPARC$^{+/+}$ mice.

In the absence of SPARC, we also observed a significantly increased in PCNA expression in the hepatic parenchyma after HFD-feeding for 16 weeks. The transcriptomic analysis of hepatic tissue of $SPARC^{+/+}$ and $SPARC^{-/-}$ mice revealed that the differential upregulated genes in $SPARC^{-/-}$ are linked with DNA maintenance, replication and diverse metabolic pathways including those related with lipid metabolism. This data suggests that in the absence of SPARC, lipid metabolic alterations associated with a hepatocellular proliferative stimulus might promote HCC progression. To further understand the correlation between lipid metabolism and SPARC we analyzed human HCC gene expression database comparing differential gene expression from tumor and non-tumor tissue. Our results indicate that SPARC gene expression negatively correlated with expression of genes related with lipid metabolism and metabolic processes. We did not find a negative correlation with genes involved in cell cycle and replication, but when we tested a signature of 207 genes that negatively correlate with SPARC expression and mostly related with metabolic processes we observed that patients with high expression levels of these genes a have poor overall survival. In line with this, Budhu *et al*. identified a lipogenic network based on gene expression and metabolic profile analysis with a strong association with HCC progression and poor patient outcomes [57]. One limitation of our analysis was that gene expression database used in our analysis contains information of patients from different etiologies, and not only from NAFLD-related HCC.

In summary, this work described a key role of SPARC in lipid hepatic metabolism and demonstrated that the increased hepatic lipid deposits in $SPARC^{-/-}$ mice is associated to hepatocarcinogenesis in a NAFLD-HCC murine model. We also demonstrated that SPARC expression negatively correlated with the expression of lipid metabolism-related genes in patients with HCC and poor survival.

All in all, this work strongly suggests that SPARC has a critical role in lipid metabolic regulation, and that the absence of SPARC is clearly associated with higher lipid accumulations within hepatocytes, and with increased HCC development. Further investigations are needed to elucidate the intimate mechanisms by which SPARC interacts with key lipid metabolic proteins.

Acknowledgements

We thank Guillermo Gaston, Franco Puebla, Santiago Cabrera and Paula Rosello for expert technical assistance.

Bibliography

1. Forner A, Reig M, Bruix J. Hepatocellular carcinoma. *Lancet*. 2018;391(10127):1301-1314. doi:10.1016/S0140-6736(18)30010-2
2. Yang JD, Hainaut P, Gores GJ, Amadou A, Plymoth A, Roberts LR. A global view of hepatocellular carcinoma: trends, risk, prevention and management. *Nat Rev Gastroenterol Hepatol*. 2019;16(10):589-604. doi:10.1038/s41575-019-0186-y
3. Cotter TG, Rinella M. Nonalcoholic Fatty Liver Disease 2020: The State of the Disease. *Gastroenterology*. 2020;158(7):1851-1864. doi:10.1053/j.gastro.2020.01.052
4. Younossi Z, Tacke F, Arrese M, et al. Global Perspectives on Nonalcoholic Fatty Liver Disease and Nonalcoholic Steatohepatitis. *Hepatology*. 2019;69(6):2672-2682. doi:10.1002/hep.30251
5. Angulo P, Keach JC, Batts KP, Lindor KD. Independent predictors of liver fibrosis in patients with nonalcoholic steatohepatitis. *Hepatology*. 1999;30(6):1356-1362. doi:10.1002/hep.510300604
6. Anstee QM, Reeves HL, Kotsiliti E, Govaere O, Heikenwalder M. From NASH to HCC: current concepts and future challenges. *Nat Rev Gastroenterol Hepatol*. 2019;16(7):411-428. doi:10.1038/s41575-019-0145-7
7. Snaebjornsson MT, Janaki-Raman S, Schulze A. Greasing the Wheels of the Cancer Machine: The Role of Lipid Metabolism in Cancer. *Cell Metab*. 2020;31(1):62-76. doi:10.1016/j.cmet.2019.11.010
8. Boroughs LK, Deberardinis RJ. Metabolic pathways promoting cancer cell survival and growth. *Nat Cell Biol*. 2015;17(4):351-359. doi:10.1038/ncb3124
9. Berger NA. Obesity and cancer pathogenesis. *Ann N Y Acad Sci*. 2014;1311(1):57-76. doi:10.1111/nyas.12416
10. Fabbrini E, Sullivan S, Klein S. Obesity and nonalcoholic fatty liver disease: Biochemical,

metabolic, and clinical implications. *Hepatology*. 2010;51(2):679-689. doi:10.1002/hep.23280

11. Nakagawa H, Hayata Y, Kawamura S, Yamada T, Fujiwara N, Koike K. Lipid metabolic reprogramming in hepatocellular carcinoma. *Cancers (Basel)*. 2018;10(11):10-15. doi:10.3390/cancers10110447
12. Calvisi DF, Wang C, Ho C, et al. Increased lipogenesis, induced by AKT-mTORC1-RPS6 signaling, promotes development of human hepatocellular carcinoma. *Gastroenterology*. 2011;140(3):1071-1083.e5. doi:10.1053/j.gastro.2010.12.006
13. Lally JSV, Ghoshal S, DePeralta DK, et al. Inhibition of Acetyl-CoA Carboxylase by Phosphorylation or the Inhibitor ND-654 Suppresses Lipogenesis and Hepatocellular Carcinoma. *Cell Metab*. 2019;29(1):174-182.e5. doi:10.1016/j.cmet.2018.08.020
14. Nelson ME, Lahiri S, Chow JDY, et al. Inhibition of hepatic lipogenesis enhances liver tumorigenesis by increasing antioxidant defence and promoting cell survival. *Nat Commun*. 2017;8(1):1-11. doi:10.1038/ncomms14689
15. Tang Z, Kang B, Li C, Chen T, Zhang Z. GEPIA2: an enhanced web server for large-scale expression profiling and interactive analysis. *Nucleic Acids Res*. 2019;47(W1):W556-W560. doi:10.1093/nar/gkz430
16. Li N, Zhou Z Sen, Shen Y, et al. Inhibition of the sterol regulatory element-binding protein pathway suppresses hepatocellular carcinoma by repressing inflammation in mice. *Hepatology*. 2017;65(6):1936-1947. doi:10.1002/hep.29018
17. Wen YA, Xiong X, Zaytseva YY, et al. Downregulation of SREBP inhibits tumor growth and initiation by altering cellular metabolism in colon cancer article. *Cell Death Dis*. 2018;9(3):1-14. doi:10.1038/s41419-018-0330-6
18. Bradshaw AD, Sage EH. SPARC, a matricellular protein that functions in cellular differentiation and tissue response to injury. *J Clin Invest*. 2001;107(9):1049-1054. http://www.ncbi.nlm.nih.gov/entrez/query.fcgi?cmd=Retrieve&db=PubMed&dopt=Citation&list_uids=11342565.
19. Trombetta-Esilva J, Bradshaw AD. The Function of SPARC as a Mediator of Fibrosis. *Open Rheumatol J*. 2012;6:146-155. doi:10.2174/1874312901206010146

20. Camino AM, Atorrasagasti C, Maccio D, et al. Adenovirus-mediated inhibition of SPARC attenuates liver fibrosis in rats. *J Gene Med*. 2008;10(9):993-1004. doi:10.1002/jgm.1228

21. Atorrasagasti C, Peixoto E, Aquino JB, et al. Lack of the matricellular protein SPARC (secreted protein, acidic and rich in cysteine) attenuates liver fibrogenesis in mice. *PLoS One*. 2013;8(2):e54962. doi:10.1371/journal.pone.0054962

22. Atorrasagasti C, Aquino JB, Hofman L, et al. SPARC downregulation attenuates the profibrogenic response of hepatic stellate cells induced by TGF-ß1 and PDGF. *Am J Physiol - Gastrointest Liver Physiol*. 2011;300(5). doi:10.1152/ajpgi.00316.2010

23. Mazzolini G, Atorrasagasti C, Onorato A, et al. SPARC expression is associated with hepatic injury in rodents and humans with non-alcoholic fatty liver disease. *Sci Rep*. 2018;8(1):725. doi:10.1038/s41598-017-18981-9

24. Atorrasagasti C, Onorato A, Gimeno ML, et al. SPARC is required for the maintenance of glucose homeostasis and insulin secretion in mice. *Clin Sci*. 2019;133(2):351-365. doi:10.1042/CS20180714

25. Atorrasagasti C, Malvicini M, Aquino JB, et al. Overexpression of SPARC obliterates the in vivo tumorigenicity of human hepatocellular carcinoma cells. *Int J Cancer*. 2010;126(11):2726-2740. doi:10.1002/ijc.24966

26. Henkel A, Green RM. The unfolded protein response in fatty liver disease. *Semin Liver Dis*. 2013;33(4):321-329. doi:10.1055/s-0033-1358522

27. Chern YJ, Wong JCT, Cheng GSW, et al. The interaction between SPARC and GRP78 interferes with ER stress signaling and potentiates apoptosis via PERK/eIF2α and IRE1α/XBP-1 in colorectal cancer. *Cell Death Dis*. 2019;10(7):1-14. doi:10.1038/s41419-019-1687-x

28. Aoi W, Naito Y, Takagi T, et al. A novel myokine, secreted protein acidic and rich in cysteine (SPARC), suppresses colon tumorigenesis via regular exercise. *Gut*. 2013;62(6):882-889. doi:10.1136/gutjnl-2011-300776

29. Melouane A, Carbonell A, Yoshioka M, Puymirat J, St-Amand J. Implication of SPARC in the modulation of the extracellular matrix and mitochondrial function in muscle cells. *PLoS One*. 2018;13(2). doi:10.1371/journal.pone.0192714

30. So B, Kim H-J, Kim J, Song W. Exercise-induced myokines in health and metabolic diseases. *Integr Med Res*. 2014;3(4):172-179. doi:10.1016/j.imr.2014.09.007

31. Song H, Guan Y, Zhang L, Li K, Dong C. SPARC interacts with AMPK and regulates GLUT4 expression. *Biochem Biophys Res Commun*. 2010;396(4):961-966. doi:10.1016/j.bbrc.2010.05.033

32. Ghanemi A, Melouane A, Yoshioka M, St-Amand J. Secreted protein acidic and rich in cysteine and bioenergetics: Extracellular matrix, adipocytes remodeling and skeletal muscle metabolism. *Int J Biochem Cell Biol*. 2019;117:105627. doi:10.1016/j.biocel.2019.105627

33. Fujii M, Shibazaki Y, Wakamatsu K, et al. A murine model for non-alcoholic steatohepatitis showing evidence of association between diabetes and hepatocellular carcinoma. *Med Mol Morphol*. 2013;46(3):141-152. doi:10.1007/s00795-013-0016-1

34. Fiore EJ, Bayo JM, Garcia MG, et al. Mesenchymal stromal cells engineered to produce IGF-I by recombinant adenovirus ameliorate liver fibrosis in mice. *Stem Cells Dev*. 2015;24(6):791-801. doi:10.1089/scd.2014.0174

35. Kleiner DE, Brunt EM, Van Natta M, et al. Design and validation of a histological scoring system for nonalcoholic fatty liver disease. *Hepatology*. 2005;41(6):1313-1321. doi:10.1002/hep.20701

36. Mehlem A, Hagberg CE, Muhl L, Eriksson U, Falkevall A. Imaging of neutral lipids by oil red O for analyzing the metabolic status in health and disease. *Nat Protoc*. 2013;8(6):1149-1154. doi:10.1038/nprot.2013.055

37. Nath A, Li I, Roberts LR, Chan C. Elevated free fatty acid uptake via CD36 promotes epithelial-mesenchymal transition in hepatocellular carcinoma. *Sci Rep*. 2015;5(April):1-19. doi:10.1038/srep14752

38. Weber K, Casali C, Gaveglio V, et al. TAG synthesis and storage under osmotic stress. A requirement for preserving membrane homeostasis in renal cells. *Biochim Biophys Acta - Mol Cell Biol Lipids*. 2018;1863(9):1108-1120. doi:10.1016/j.bbalip.2018.06.012

39. Chen J, Bardes EE, Aronow BJ, Jegga AG. ToppGene Suite for gene list enrichment analysis and candidate gene prioritization. *Nucleic Acids Res*. 2009;37(SUPPL. 2):305-311. doi:10.1093/nar/gkp427

40. Liao Y, Smyth GK, Shi W. The R package Rsubread is easier, faster, cheaper and better for alignment and quantification of RNA sequencing reads. *Nucleic Acids Res*. 2019;47(8):e47-e47. doi:10.1093/nar/gkz114

41. Chen EY, Tan CM, Kou Y, et al. Enrichr: Interactive and collaborative HTML5 gene list enrichment analysis tool. *BMC Bioinformatics*. 2013;14. doi:10.1186/1471-2105-14-128

42. Nie J, Sage EH. SPARC functions as an inhibitor of adipogenesis. *J Cell Commun Signal*. 2009;3(3-4):247-254. doi:10.1007/s12079-009-0064-4

43. Duarte FO, Gomes-Gatto C do V, Oishi JC, et al. Physical training improves visceral adipose tissue health by remodelling extracellular matrix in rats with estrogen absence: a gene expression analysis. *Int J Exp Pathol*. 2017;98(4):203-213. doi:10.1111/iep.12237

44. Yahagi N, Shimano H, Hasegawa K, et al. Co-ordinate activation of lipogenic enzymes in hepatocellular carcinoma. *Eur J Cancer*. 2005;41(9):1316-1322. doi:10.1016/j.ejca.2004.12.037

45. Brown MS, Goldstein JL. The SREBP pathway: Regulation of cholesterol metabolism by proteolysis of a membrane-bound transcription factor. *Cell*. 1997;89(3):331-340. doi:10.1016/S0092-8674(00)80213-5

46. Horton JD, Goldstein JL, Brown MS. SREBPs: activators of the complete program of cholesterol and fatty acid synthesis in the liver. *J Clin Invest*. 2002;109(9):1125-1131. doi:10.1172/jci15593

47. Melouane A, Yoshioka M, Kanzaki M, St-Amand J. Sparc, an EPS-induced gene, modulates the extracellular matrix and mitochondrial function via ILK/AMPK pathways in C2C12 cells. *Life Sci*. 2019;229:277-287. doi:10.1016/j.lfs.2019.05.070

48. Loubière C, Goiran T, Laurent K, Djabari Z, Tanti JF, Bost F. Metformin-induced energy deficiency leads to the inhibition of lipogenesis in prostate cancer cells. *Oncotarget*. 2015;6(17):15652-15661. doi:10.18632/oncotarget.3404

49. Saito T, Muramatsu M, Ishii Y, et al. Pathophysiological analysis of the progression of hepatic lesions in STAM mice. *Physiol Res*. 2017;66(5):791-799. doi:10.33549/physiolres.933592

50. Saito K, Uebanso T, Maekawa K, et al. Characterization of hepatic lipid profiles in a mouse

model with nonalcoholic steatohepatitis and subsequent fibrosis. *Sci Rep*. 2015;5(1):12466. doi:10.1038/srep12466

51. Nie J, Sage EH. SPARC inhibits adipogenesis by its enhancement of beta-catenin signaling. *J Biol Chem*. 2009;284(2):1279-1290. doi:10.1074/jbc.M808285200

52. Melouane A, Carbonell A, Yoshioka M, Puymirat J, St-Amand J. Implication of SPARC in the modulation of the extracellular matrix and mitochondrial function in muscle cells. *PLoS One*. 2018;13(2):e0192714. doi:10.1371/journal.pone.0192714

53. Yamashita T, Honda M, Takatori H, et al. Activation of lipogenic pathway correlates with cell proliferation and poor prognosis in hepatocellular carcinoma. *J Hepatol*. 2009;50(1):100-110. doi:10.1016/j.jhep.2008.07.036

54. Li Y, Xu S, Mihaylova MM, et al. AMPK phosphorylates and inhibits SREBP activity to attenuate hepatic steatosis and atherosclerosis in diet-induced insulin-resistant mice. *Cell Metab*. 2011;13(4):376-388. doi:10.1016/j.cmet.2011.03.009

55. Zaidi N, Lupien L, Kuemmerle NB, Kinlaw WB, Swinnen J V., Smans K. Lipogenesis and lipolysis: The pathways exploited by the cancer cells to acquire fatty acids. *Prog Lipid Res*. 2013;52(4):585-589. doi:10.1016/j.plipres.2013.08.005

56. Ridolfi R, Amaducci L, Derni S, Fabbri L, Innocenti MP, Vignutelli P. Chemotherapy with 5-fluorouracil and streptozotocin in carcinoid tumors of gastrointestinal origin: Experiences with 13 patients. *J Chemother*. 1991;3(5):328-331. doi:10.1080/1120009X.1991.11739114

57. Budhu A, Roessler S, Zhao X, et al. Integrated metabolite and gene expression profiles identify lipid biomarkers associated with progression of hepatocellular carcinoma and patient outcomes. *Gastroenterology*. 2013;144(5). doi:10.1053/j.gastro.2013.01.054

Figure legends

Table 1: *Clinical characteristics of patients with HCC in the TCGA and ICGC cohorts.*

Figure 1: *Increased hepatic triglycerides deposit in SPARC$^{-/-}$ mice in an age-dependent manner*

A) Oil Red O staining of liver sections from SPARC$^{+/+}$ and SPARC$^{-/-}$ mice fed with chow diet for 6, 18, 26 and 30 weeks. Image magnification: 100X. **B)** Liver triglycerides (TG) levels in SPARC$^{+/+}$and SPARC$^{-/-}$ mice were measured at 6, 10, 14, 18, 26 and 30 weeks (n= 3). Two independent assays were performed. *p<0.05; Mann-Whitney test.

Figure 2: *SPARC inhibition promotes an increased neutral lipid deposits in hepatocytes.*

A) Representative images of primary hepatocyte culture from SPARC$^{+/+}$ and SPARC$^{-/-}$ mice stained with Oil Red O. Cells were exposed or not to 0.25 or 0.5 mM free fatty acids for 12h (FFA: oleate acid +palmitic acid, 2:1 ratio). Image magnification: 400X. **B)** Quantification of Oil Red O staining in primary hepatocyte culture after liberating colorant from cells by adding isopropyl alcohol and measuring in a spectrophotometer at 510 nm. Three independent assays were performed. *p<0.05; Mann-Whitney test. **C)** Chromatography determination of endogenous triglycerides (GL-TGL) and endogenous glycerophospholipid (GPL) in primary hepatocyte culture from SPARC$^{+/+}$ and SPARC$^{-/-}$ mice, incubated or not with 0.5mM FFA. **D)** SPARC mRNA expression detected by qPCR in HepG2 cell line infected with AdasSPARC, Adβgal or left uninfected. Three independent assays were performed. Data are represented as mean ± SEM. *p<0.05, **p<0.01; Kruskal-Wallis test with Dunn's post test. **E)** Quantification of % positive Oil Red O staining area in HepG2 cell line, incubated or not with 0.5 or 1mM FFA for 12 h. B. Three independent assays were performed. *p<0.05, *p<0.01; Kruskal-Wallis test with Dunn's post test.

Figure 3: *The absence of SPARC in primary culture hepatocytes is associated with increased de novo triglyceride synthesis, induction of key lipid metabolism genes, and with hepatocyte survival and resistance to apoptosis.*

A) Primary hepatocyte culture from SPARC$^{+/+}$ and SPARC$^{-/-}$ mice were incubated or not with 0.5 mM free fatty acids (FFA: oleate acid +palmitic acid, 2:1 ratio), then TG synthesis was determined

by incubation with ^{14}C-glycerol for 1, 2 and 3 h followed by total lipid extraction, TG chromatography isolation and analysis of 14C incorporation measured by liquid scintillation counting. Data represent the mean ± SEM for 3 replicates per group. Three independent assays were performed *p<0.05; ****p<0.0001; Tukey's multiple comparisons test. **B)** Primary hepatocyte culture from SPARC$^{+/+}$ and SPARC$^{-/-}$ mice were incubated or not with 0.5 mM FFA in the presence or absence of 5 μg/ml of TOFA for 16 h. Quantification of Oil Red O staining after liberating colorant from cells by adding isopropyl alcohol and measuring in a spectrophotometer at 510 nm. ΔI, incremented factor, calculate as absorbance obtained when cells were treated with FFA/absorbance without FFA treatment. Three independent assays were performed. **C)** mRNA expression of CD36, FABP4, FABP5, ACC1, FASN1, SREBP1, LXRα, PPARγ2, PPARα, LIPIN1, ACADSB, CPT1 and ACOX1 detected by qPCR in primary hepatocyte culture derived from SPARC$^{+/+}$ and SPARC$^{-/-}$ mice. n=2 for SPARC$^{+/+}$ and SPARC$^{-/-}$. The data is represented as mean ± SEM. SPARC$^{+/+}$ vs. SPARC$^{-/-}$ *p<0.05; **p<0.01; Mann Whitney test. **D)** Viability of SPARC$^{+/+}$ and SPARC$^{-/-}$ hepatocyte primary culture treated with 0.25, 0.5 and 1 mM FFA for 12 h was assessed by MTT assay. Three independent assays were performed. The data is represented as mean ± SEM. SPARC$^{+/+}$ vs SPARC$^{-/-}$ *p<0.05; Kruskal-Wallis test with Dunn's post test. **E)** Proliferation of SPARC$^{+/+}$ and SPARC$^{-/-}$ hepatocyte primary culture treated with 0.5 and 1 mM FFA assessed by [methyl 3H] thymidine incorporation. The data is represented as mean ± SEM. Kruskal-Wallis test with Dunn's post test. **F)** Apoptosis of SPARC$^{+/+}$ and SPARC$^{-/-}$ hepatocyte primary culture was assessed by acridine orange-ethidium bromide staining after 1 mM FFA or without incubation (-FFA). Representative fluorescent images of 4 experimental groups are shown. Image magnification: 400X. Percentage of alive cells is shown. SPARC$^{+/+}$ -FFA vs SPARC$^{+/+}$ +1 mM FFA *p<0.05; Kruskal-Wallis test with Dunn's post test.

Figure 4: *Enhanced nuclear translocation of SREBP1 in SPARC$^{-/-}$ hepatocytes.*

A) Inmunofluorescence analysis of SREBP1c nuclear translocation in hepatocyte primary culture derived from SPARC$^{+/+}$ and SPARC$^{-/-}$ mice. Cells were exposed or not to 0.5 mM FFA for 12 h and immunostained with anti-SREBP1c antibody (green) and DAPI (blue). Image magnification: 400X. **B)** Quantification of the percentage of positive nuclear signal for immunofluorescence anti-SREBP1 in hepatocytes, using image analysis. n=3 culture wells per group. *p<0.05, **p<0.01; Kruskal-Wallis test with Dunn's post test. **C)** Representative immunofluorescence images of

HepG2 cells infected with AdasSPARC, Adβgal or left uninfected. Cells were stained with anti-SREBP1c antibody (red) and DAPI (blue). Image magnification: 200X. **D)** Quantification of the percentage of positive cytoplasmic signal for anti-SREBP1c in HepG2, using image analysis. n=3 culture wells per group. *p<0.05; Kruskal-Wallis test with Dunn's post test. **E)** Immunohistochemistry for SREBP1c in liver parenchyma of $SPARC^{+/+}$ and $SPARC^{-/-}$ mice. Magnification: 400X. Quantification of SREBP1c positive nucleus. n=3 mice per group. Ten random fields were analyzed for each group (400X magnification). $SPARC^{-/-}$ vs. $SPARC^{+/+}$ ***p<0.001, Mann-Whitney test. **F)** Western blot analysis of p-AMPK on primary hepatocyte culture from 18-week-old $SPARC^{+/+}$ and $SPARC^{-/-}$ mice**;** α-Tubulin was used as loading control. Lanes for each detection are in their original order and correspond to the same gel. **G)** Inmunofluorescence analysis of SREBP1c nuclear translocation in hepatocyte primary culture derived from $SPARC^{-/-}$ mice treated 2mM with metformin for 24 h. Cells were immunostained with anti-SREBP1c antibody (green) and DAPI (blue).

Figure 5: *SPARC low expression associates with altered lipid metabolic profile in HCC.*

A) RNA sequencing (RNA-seq) data expression analysis of HCC using TCGA (in blue) and ICGC (in red) databases. Analysis of genes correlating with SPARC expression in 2 groups: those with strong positive correlation (Pearson coefficient ≥0.6, fdr ≤ 0.05) and those with a moderate negative correlation (Pearson coefficient between -0.6 and -0.3, fdr ≤ 0.05). Venn diagram of TCGA and ICGC genes in each group. **B)** Gene ontology analysis of positive correlating genes. Graph shows number of genes (right axis, column bars) and q-value FDR B&H (left axis, dots). **C)** Gene ontology analysis of negatively correlating genes. **D)** Patients with high expression of a gene signature consisting of 207 genes that negatively correlate with SPARC (red line) have poor survival in comparison with those expressing low levels (blue line). Levels were defined by top and bottom quartiles. The association between expression in HCC and the survival time was analyzed with Kaplan-Meier survival analysis.

Figure 6: *The absence of SPARC is associated with increased steatosis but low inflammation degree and fibrosis.*

A) Representative H&E- stained images of liver sections from streptozotocin (SZT)- treated SPARC$^{+/+}$ and SPARC$^{-/-}$ mice after feeding with chow diet (CD) or high fat diet (HFD) diet for 8 weeks. Yellow arrows indicate presence of inflammatory infiltrate, blue arrows indicate lipid macrovesicles and green arrows indicate ballooning of hepatocytes. Image magnification: 200X. **B)** NAFLD activity score (NAS) analyzing steatosis, inflammation, and ballooning in SPARC$^{+/+}$ mice in comparison with SPARC$^{-/-}$ mice after 8 weeks of feeding with CD or HFD (n= 3-5 mice per group). Data are represented as mean ± SD. * compared diet effect (CD vs HFD) in both SPARC$^{+/+}$ and SPARC$^{-/-}$ mice, $^{\sigma}$ compared genotype in both CD and HFD; *,$^{\sigma}$p<0.1; **,$^{\sigma\sigma}$p<0.01 and ****p<0.0001; Mann Whitney test. **C)** Hepatic SPARC mRNA expression detected by qPCR in SZT-treated SPARC$^{+/+}$ CD and HFD mice, after 8 weeks of feeding. n=2 for SPARC$^{+/+}$ CD and n=3 for SPARC$^{+/+}$ HFD. Data are represented as mean ± SEM. **p<0.01, Mann Whitney test. **D)** Hepatic mRNA expression of IL6, IP10, TNFα, NLRP3, CASP-1 and IL1β detected by qPCR in CD or HFD-fed SZT-treated SPARC$^{+/+}$ and SPARC$^{-/-}$mice (n=3 mice per group). The data is represented as mean ± SEM. *p<0.05; **p<0.01; ***p<0.001; ****p<0.0001; Kruskal-Wallis test with Dunn's post test. **E)** Representative images of Sirius red staining of liver sections from SZT-treated SPARC$^{+/+}$ and SPARC$^{-/-}$ mice after feeding with CD or HFD for 8 weeks. Arrows indicate collagen deposition. Magnification: 200X. **F)** Quantification of Sirius red-positive areas using image analysis. n= 6–8 mice per group. ****p<0.0001; Kruskal-Wallis test with Dunn's post test.

Figure 7: *The absence of SPARC is associated with increased HCC incidence and an exacerbated proliferative profile*

A) Representative H&E-stained images of liver sections from streptozotocin (SZT)- treated SPARC$^{+/+}$ and SPARC$^{-/-}$ mice after feeding with high fat diet (HFD) diet for 16 weeks (n=6-8 mice per group). Dotted black lines delimit a liver tumor. Image magnification: 200X. **B)** Macroscopic photographs of liver of SZT-treated SPARC$^{+/+}$ and SPARC$^{-/-}$ mice after 16 weeks of feeding with HFD. White discontinuous circles indicate tumors. **C)** Quantification of liver tumors observed macroscopically in the liver at sacrifice (tumors with a volume greater than 1 mm^3 were counted). n=19 for SPARC$^{+/+}$ and n=13 for SPARC$^{-/-}$. The data is represented as mean ± SD. **D)** Measure of tumor volume, n=19 for SPARC$^{+/+}$ and n=13 for SPARC$^{-/-}$. The data is represented as mean ± SD. SPARC$^{-/-}$ HFD vs SPARC$^{+/+}$ HFD ****p<0.0001; Mann-Whitney test. **E)** Incidence of liver tumors in SZT-treated SPARC$^{+/+}$ and SPARC$^{-/-}$ mice fed with HFD, for tumors < and >

than 1mm. n=19 for $SPARC^{+/+}$ and n=13 for $SPARC^{-/-}$. **F)** Immunohistochemistry for proliferating cell nuclear antigen (PCNA) in liver parenchyma of SZT-treated $SPARC^{+/+}$ and $SPARC^{-/-}$ HFD-fed mice. Magnification: 200X. **G)** PCNA positive nucleus quantification. n=8 mice per group. Ten random fields were analyzed for each group (200X magnification). $SPARC^{-/-}$ HFD vs $SPARC^{+/+}$ HFD *$p<0.05$, Mann-Whitney test. **H)** RNA sequencing (RNA-seq) analysis from hepatic tissue (tumoral and non-tumoral tissue was included) of SZT-treated $SPARC^{+/+}$ and $SPARC^{-/-}$ 16 weeks HFD-fed mice. Enriched pathway analysis of DEGs between $SPARC^{+/+}$ and $SPARC^{-/-}$ mice. Enriched pathway analysis of the 302 SZT-treated $SPARC^{-/-}$ upregulated genes. Selection criteria for upregulated genes was established by a p-value ≤ 0.05 and fold change (FC)≥ 2. n=2 samples per group. The x axis shows the enrichment significance presented with q value.

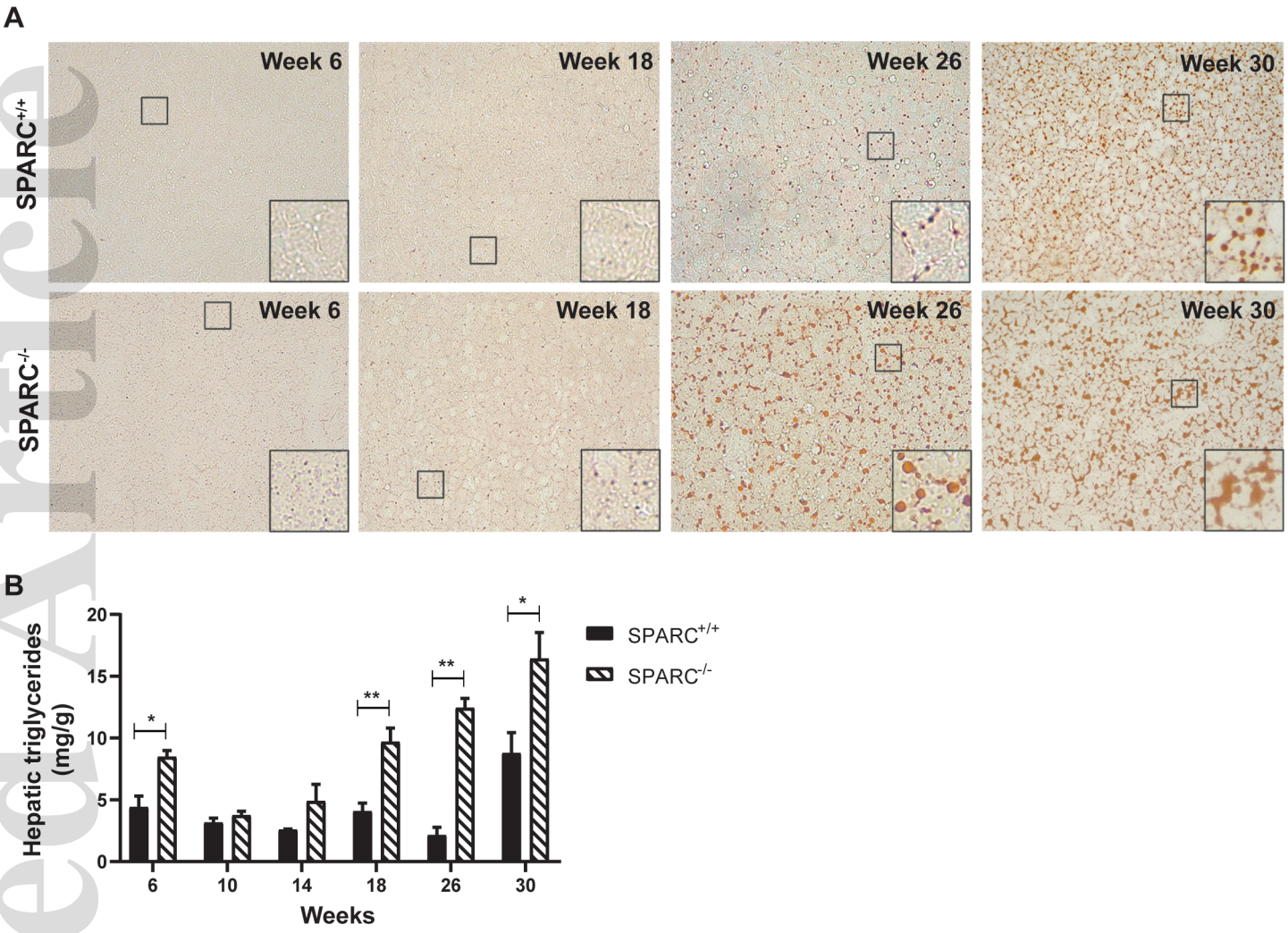

liv_14857_f1.tif

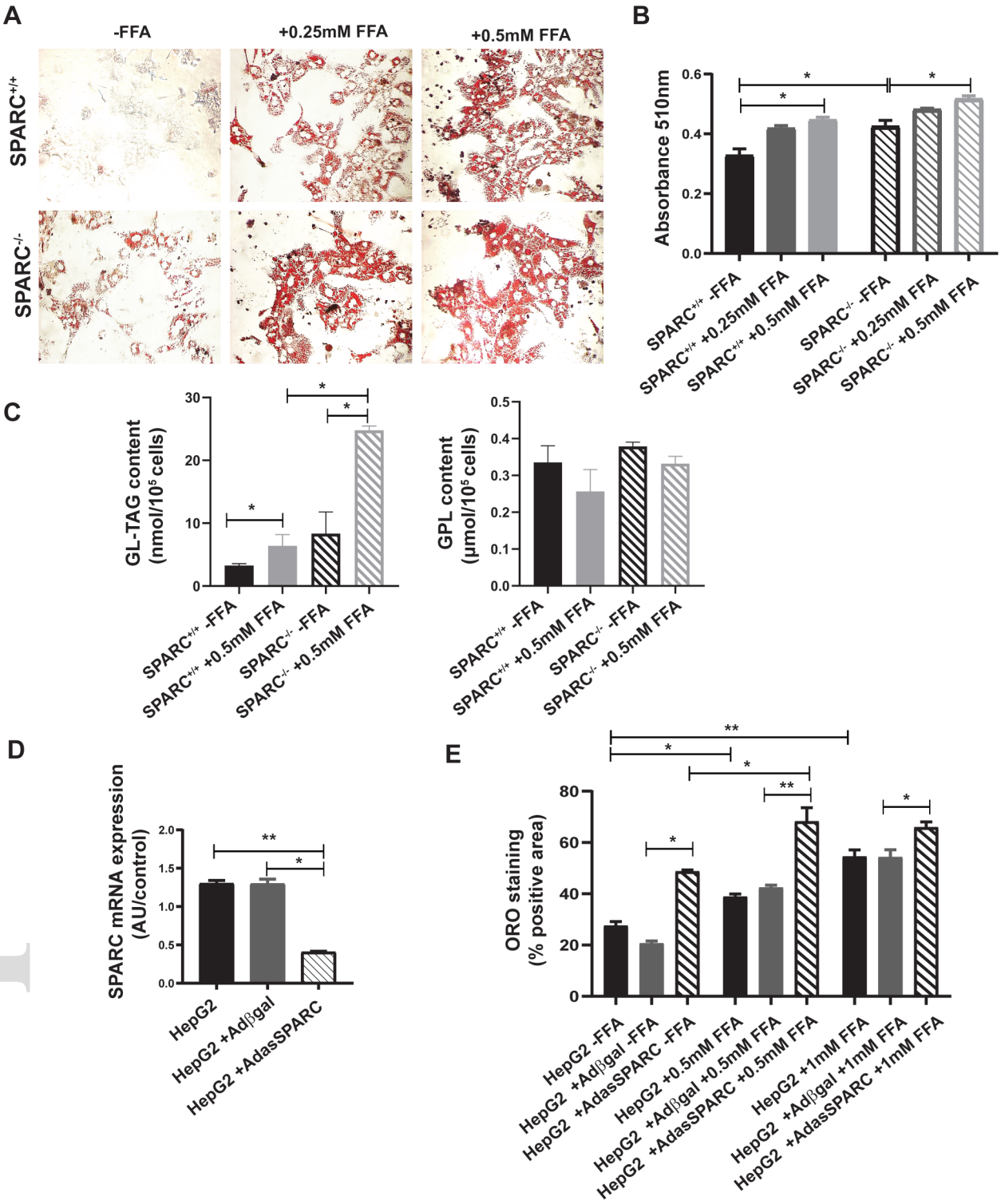

liv_14857_f2.tif

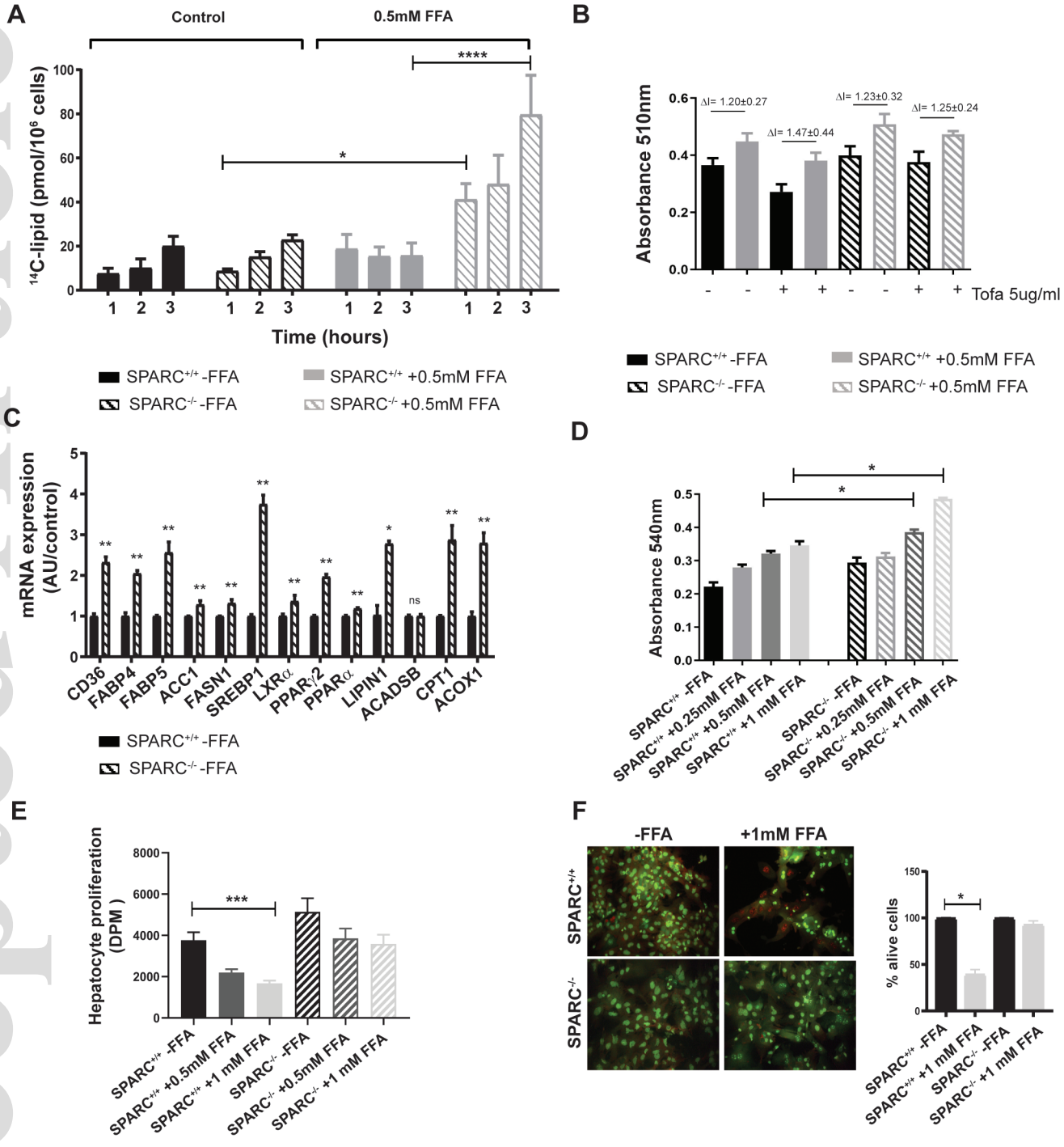

liv_14857_f3.tif

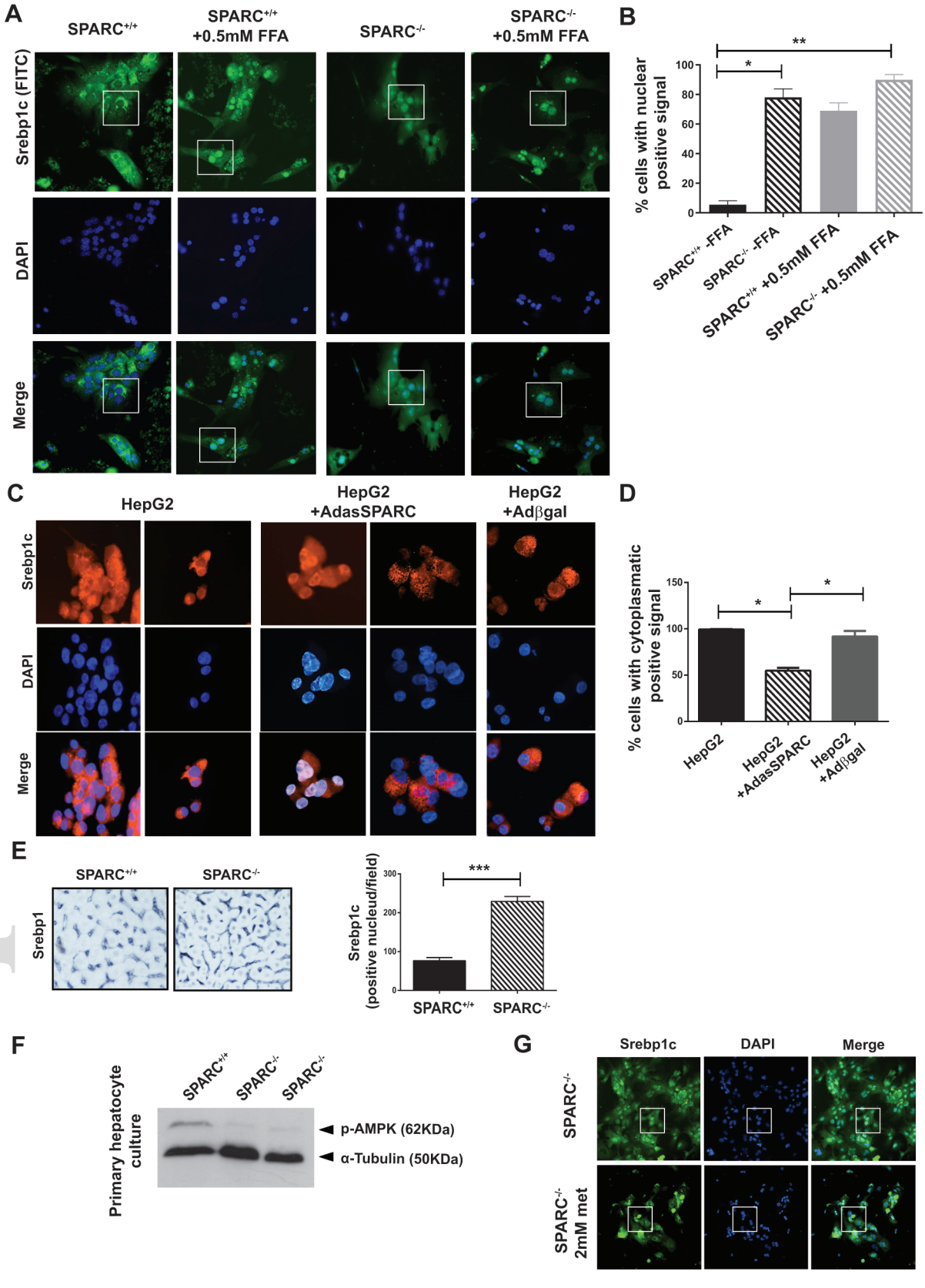

liv_14857_f4.tif

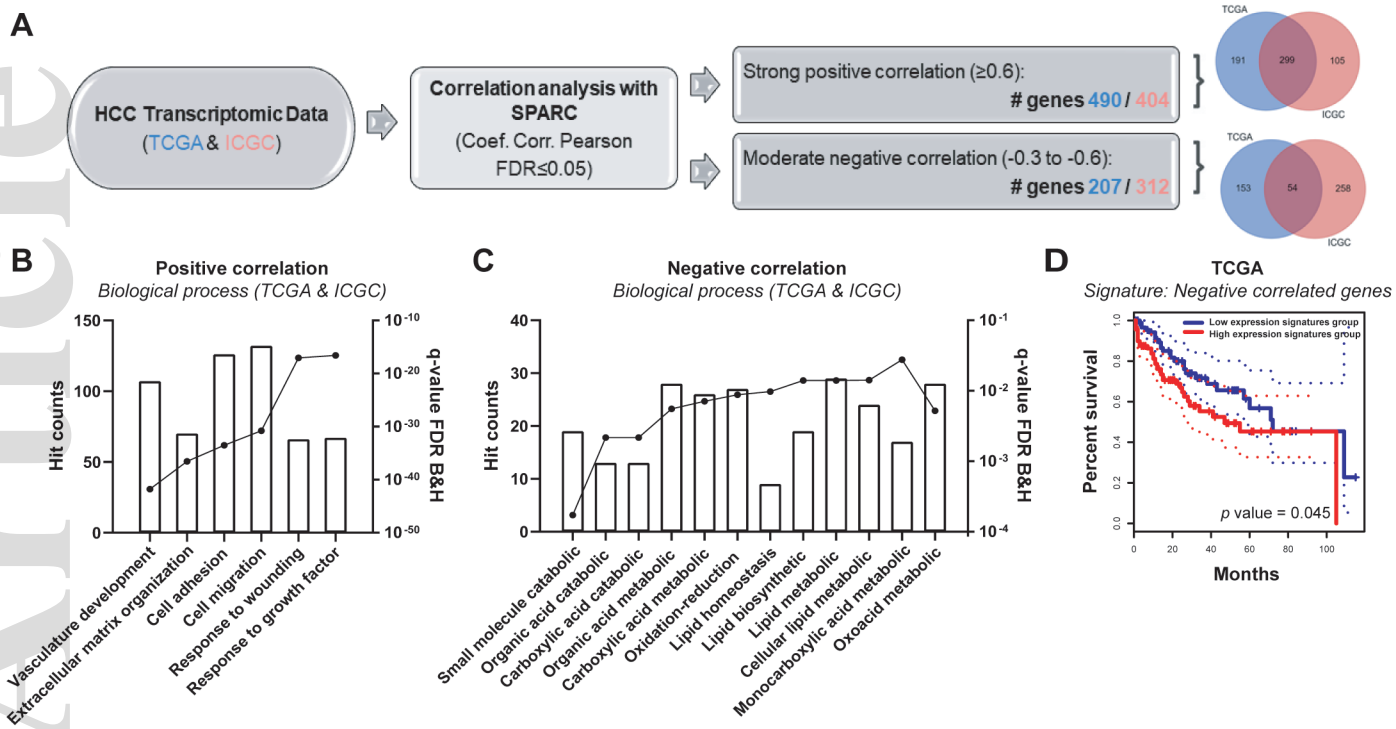

liv_14857_f5.tif

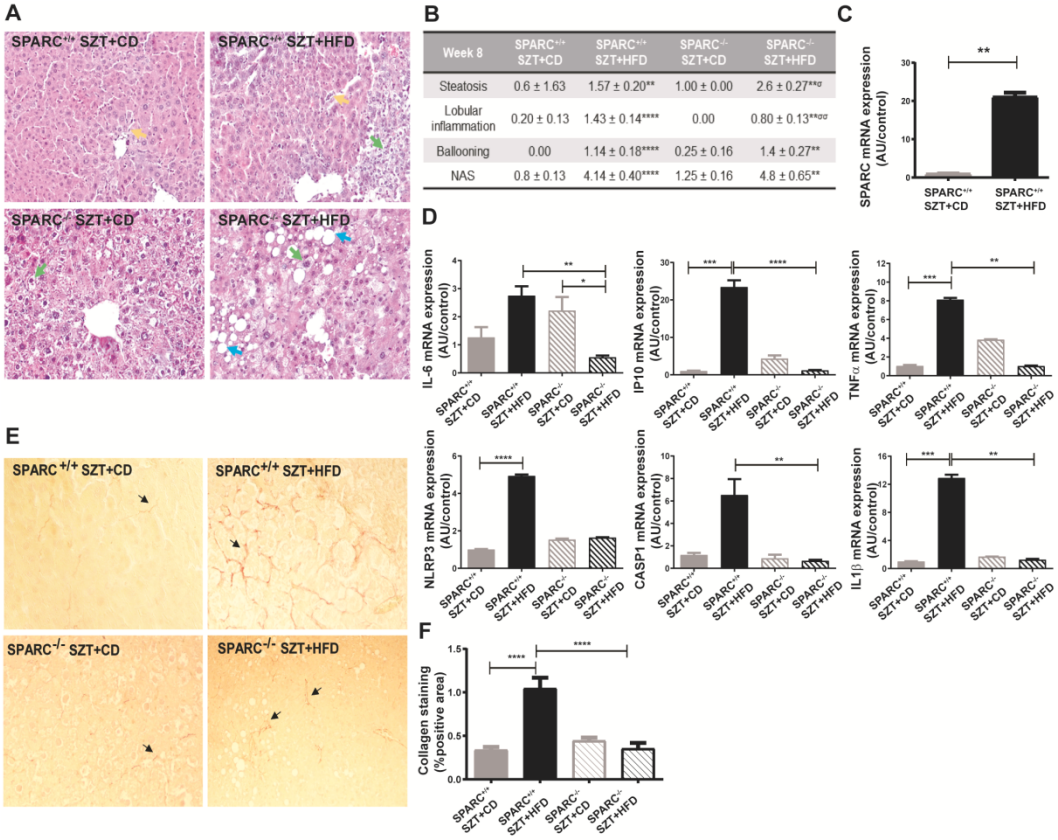

Week 8	SPARC+/+ SZT+CD	SPARC+/+ SZT+HFD	SPARC-/- SZT+CD	SPARC-/- SZT+HFD
Steatosis	0.6 ± 1.63	1.57 ± 0.20**	1.00 ± 0.00	2.6 ± 0.27**α
Lobular inflammation	0.20 ± 0.13	1.43 ± 0.14****	0.00	0.80 ± 0.13**αα
Ballooning	0.00	1.14 ± 0.18****	0.25 ± 0.16	1.4 ± 0.27**
NAS	0.8 ± 0.13	4.14 ± 0.40****	1.25 ± 0.16	4.8 ± 0.65**

liv_14857_f6.tif

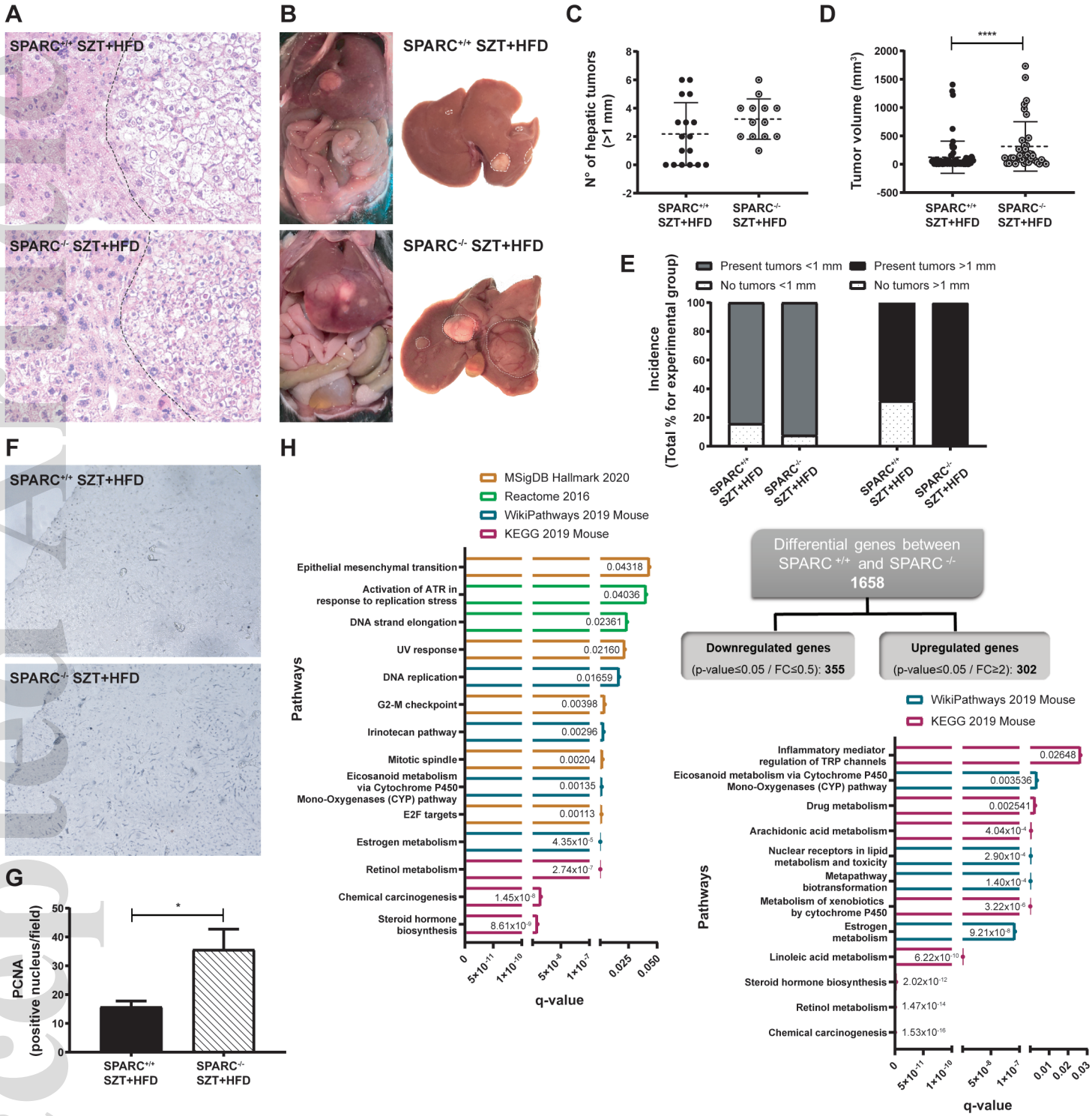

liv_14857_f7.tif

Characteristics	TCGA (n=377) n (%)	ICGC (n=203) n (%)
Age		
<50	72 (19.1)	15 (7.39)
50-65	163 (43.24)	63 (31.03)
>65	141 (37.4)	125 (61.58)
Unknown	1 (0.27)	0 (0)
Gender		
Male	255 (67.64)	153 (75.37)
Female	122 (32.36)	50 (24.63)
Race		
White	187 (49.6)	NA
Black	17 (4.51)	NA
Asian	161 (42.71)	NA
Other	2 (0.53)	NA
Unknown	10 (2.65)	NA
BMI (Body mass index)		
<18.5	21 (5.57)	NA
18.5-24.9	160 (42.44)	NA
25-29.9	92 (24.4)	NA
≥30	68 (18.04)	NA
NA	36 (9.55)	
HCC stage		
I	175 (46.42)	33 (16.26)
II	87 (23.08)	96 (47.29)
III	86 (22.81)	59 (29.06)
IV	5 (1.33)	15 (7.39)
Unknown	24 (6.37)	0 (0)
Primary etiology		
Alcohol	118 (31.3)	-
HBV infection	83 (22.02)	53 (26.11)
HBC infection	34 (9.02)	117 (57.64)
HBV and HBC infection	-	4 (1.97)
Haemochromatosis	5 (1.33)	-
Non-alcoholic fatty liver disease	12 (3.18)	-
Other or not available	32 (8.49)	29 (14.29)
No history of primary risk factor	93 (24.67)	-
Fibrosis (Ishak score)		
0 (No fibrosis)	76 (20.16)	NA
1-2 (Portal fibrosis)	31 (8.22)	NA
3-4 (Fibrous septa)	30 (7.96)	NA
5 (Nodular formation and incomplete fibrosis)	9 (2.39)	NA
6 (Cirrhosis)	72 (19.10)	NA
NA	159 (42.18)	
Fibrosis (Knodell score)		
0	NA	9 (4.43)
1	NA	27 (13.3)
2	NA	43 (21.18)
3	NA	48 (23.65)
4	NA	76 (37.44)
Vital status		
Alive	245 (64.99)	168 (82.76)
Dead	132 (35.01)	35 (17.24)

NA *for Not Available*